MOLECULAR SIMULATION, 2016
VOL. 42, NO. 16, 1364–1369
http://dx.doi.org/10.1080/08927022.2015.1114177

Taylor & Francis
Taylor & Francis Group

Multiscale dipole relaxation in dielectric materials

J. S. Hansen

DNRF Centre 'Glass and Time', Department of Science, Systems, and Models, IMFUFA, Roskilde University, Roskilde, Denmark.

ABSTRACT

Dipole relaxation from thermally induced perturbations is investigated on different length scales for dielectric materials. From the continuum dynamical equations for the polarisation, expressions for the transverse and longitudinal dipole autocorrelation functions are derived in the limit where the cross coupling between the electric field fluctuations and dipole moment fluctuations can be ignored. The peak frequencies in the spectra of the autocorrelation functions are also derived. They depend on the wave vector squared which is a fingerprint of the underlying dipole diffusion mechanism. The theoretical predictions are compared with molecular dynamics simulation results for a model dielectric material and liquid water. For the transverse dipole autocorrelation function the agreement is excellent in the limit of small wave vectors and the presence of a diffusion mechanism is confirmed. For the longitudinal direction the simulation results show that the cross coupling between the electric field and the dipole moment is non-negligible compromising the theoretical predictions. The underlying mechanism for this coupling is not clear.

ARTICLE HISTORY
Received 4 September 2015
Accepted 25 October 2015

KEYWORDS
Polarisation; dynamical response; dipole relaxation; dielectrics

1. Introduction

It is known that water tends to align near a solid surface.[1–3] Such geometrical alignment will also align the molecular dipoles and thus the system will spontaneously induce a non-zero polarisation and associated electric field.[1,4] The dielectric properties are also affected by the confinement and the permittivity features anisotropy near the solid surface.[3] For bulk water non-uniform polarisation can be achieved in the presence of a large temperature gradient.[5] Common for these systems is that the local electric field and the polarisation are vayring on a molecular length scale.

In case of a spatially varying electric field, the most general way to model the dielectric response is by introducing a wave vector-dependent dielectric susceptibility. (This transport property is also called electric susceptibility.[6]) This approach is, however, a highly coarse-grained description and may hide underlying mechanisms responsible for the response. Recently, Hansen [7] showed through non-equilibrium molecular dynamics (NEMD) simulations that the dielectric response is reduced in the presence of large polarisation gradients, that is, when the local electric field is rapidly varying with respect to spatial coordinate. The mechanism behind this reduction is the existence of an additional polarisation flux (or diffusion of dipole moment) which must exist for non-zero gradient, see also [8]. Hansen [7] further showed that the reduced response is proportional to the wave length squared of the imposed sinusoidal electrical field.

Here the multiscale dipole relaxation under equilibrium conditions is studied. The relaxation is quantified by two different autocorrelation functions, namely, the transverse and longitudinal dipole moment relaxations functions. Equilibrium molecular dynamics (EMD) simulations are carried out and the results are discussed within the theoretical framework.

2. Theory

The balance equation for the polarisation (or dipole moment density) was derived by Dahler and Scriven [9], and more recently by Hansen [7]; the latter derivation is based on the microscopic hydrodynamic operator.[10] The polarisation, $\mathbf{P}(\mathbf{r}, t)$, can be written in terms of the dipole moment per unit mass, $\mathbf{p}(\mathbf{r}, t)$, and the mass density, $\rho(\mathbf{r}, t)$, as $\mathbf{P}(\mathbf{r}, t) = \rho(\mathbf{r}, t)\mathbf{p}(\mathbf{r}, t)$. From here on the explicit time and position dependency is omitted unless it provides clarifying information. In the hydrodynamic regime of low wave vector, the balance equation for polarisation for rigid uni-axial molecules with a permanent dipole moment is given by [7]

$$\frac{\partial \rho \mathbf{p}}{\partial t} + \boldsymbol{\nabla} \cdot (\rho \mathbf{u}\mathbf{p}) = \boldsymbol{\sigma} + \frac{2\rho}{3}(\boldsymbol{\Omega} \times \mathbf{p}) - \boldsymbol{\nabla} \cdot \mathbf{R}, \tag{1}$$

where $\mathbf{u}$ is the streaming velocity, $\boldsymbol{\sigma}$ is the production term and $\boldsymbol{\Omega}$ the fluid angular velocity. $\mathbf{R}$ is the polarisation flux tensor.[7]

As mentioned above, the dynamics is investigated from relaxations in equilibrium, i.e. relaxation from thermally induced perturbations. This means that the quantities in Equation (1) are stochastic variables. Such variables can be written as the sum of the average part and fluctuating stochastic part, i.e. for some quantity A one writes $A = A_{\text{av}} + \delta A$.[6]

CONTACT J. S. Hansen jschmidt@ruc.dk

To model the dynamics, the stochastic forcing method [11] is applied. Here it is assumed that the flux $\mathbf{R}$ is equal to a set of constitutive relations relating the flux to the thermodynamic force and a stochastic forcing term that accounts for the random perturbations of the system. In equilibrium the random forcing term is uncorrelated in both time and space and has zero mean. [11] Here it is further assumed that the random force is uncorrelated with the dipole moment. Using the linear constitutive relations proposed by Hansen [7] and adding the forcing term $\delta\mathbf{R}$ one has for the polarisation flux tensor

$$\mathbf{R} = -\chi_v(\nabla\cdot\mathbf{p})\mathbf{I} - 2\chi_0\overset{os}{(\nabla\mathbf{p})} - 2\chi_r\overset{a}{(\nabla\mathbf{p})} + \delta\mathbf{R}\,. \tag{2}$$

Here χ_v, χ_0 and χ_r are the relevant transport coefficients, and $\mathbf{I}$ is the 3×3 identity tensor. Superscripts *os* and *a* indicate the traceless symmetric and anti-symmetric parts of the vector dyadic $\nabla\mathbf{p} < ... >$, respectively. Substituting Equation (2) into Equation (1) yields

$$\frac{\partial\rho\mathbf{p}}{\partial t} + \nabla\cdot(\rho\mathbf{up}) = \boldsymbol{\sigma} + \frac{2\rho}{3}(\boldsymbol{\Omega}\times\mathbf{p}) + \chi_l\nabla(\nabla\cdot\mathbf{p}) + \chi_t\nabla^2\mathbf{p} - \nabla\cdot\delta\mathbf{R}, \tag{3}$$

As a matter of convenience the new transport coefficients $\chi_t = \chi_0 + \chi_r$ and $\chi_l = \chi_v + \chi_0/3 - \chi_r$ are introduced.

Both the average dipole moment and the average angular velocity are zero in equilibrium, $\mathbf{p}_{\text{av}} = \mathbf{0}$ and $\boldsymbol{\Omega}_{\text{av}} = \mathbf{0}$, so $\mathbf{p} = \delta\mathbf{p}$ and $\boldsymbol{\Omega} = \delta\boldsymbol{\Omega}$. To first order in the fluctuations, the coupling between the angular velocity and dipole moment then vanishes as this coupling enters via a cross product and is of second order. Also, the vector dyadic between the streaming velocity and the polarisation is second order in the fluctuations. This gives, to first order,

$$\rho_{\text{av}}\frac{\partial\delta\mathbf{p}}{\partial t} = \boldsymbol{\sigma} + \chi_l\nabla(\nabla\cdot\delta\mathbf{p}) + \chi_t\nabla^2\delta\mathbf{p} - \nabla\cdot\delta\mathbf{R}. \tag{4}$$

In Fourier space for wave vector $\mathbf{k}$ this is

$$\rho_{\text{av}}\frac{\partial\widetilde{\delta\mathbf{p}}}{\partial t} = \widetilde{\boldsymbol{\sigma}} - \chi_l\mathbf{k}(\mathbf{k}\cdot\widetilde{\delta\mathbf{p}}) - \chi_t\mathbf{k}^2\widetilde{\delta\mathbf{p}} - i\mathbf{k}\cdot\widetilde{\delta\mathbf{R}}. \tag{5}$$

The production term $\boldsymbol{\sigma}$ is now addressed. The local fluctuating electric field, $\delta\mathbf{E}$, present in the dielectric material will exert a torque on the microscopic dipoles and thus affect the dipole moment dynamics. This effect is modelled into the production term. In the linear regime one has [12] $\boldsymbol{\sigma} = \rho_{\text{av}}(\kappa\delta\mathbf{E} - \delta\mathbf{p})/\tau$, where τ is the dipole relaxation time, κ is the dielectric susceptibility per unit mass. In Fourier space this is

$$\widetilde{\boldsymbol{\sigma}} = \frac{\rho_{\text{av}}}{\tau}(\kappa\widetilde{\delta\mathbf{E}} - \widetilde{\delta\mathbf{p}}). \tag{6}$$

By choosing $\mathbf{k} = (0, k_y, 0)$, one can decompose the dynamics into transverse directions, the x- and z-components of $\widetilde{\delta\mathbf{p}}$, and a longitudinal direction, the y-component, giving

$$\frac{\partial\widetilde{\delta p}_x}{\partial t} = \frac{1}{\tau}(\kappa\widetilde{\delta E}_x - \widetilde{\delta p}_x) - \nu_t k_y^2\widetilde{\delta p}_x - \frac{ik_y}{\rho_{\text{av}}}\widetilde{\delta R}_{yx} \tag{7a}$$

$$\frac{\partial\widetilde{\delta p}_y}{\partial t} = \frac{1}{\tau}(\kappa\widetilde{\delta E}_y - \widetilde{\delta p}_y) - (\nu_l + \nu_t)k_y^2\widetilde{\delta p}_y - \frac{ik_y}{\rho_{\text{av}}}\widetilde{\delta R}_{yy} \tag{7b}$$

$$\frac{\partial\widetilde{\delta p}_z}{\partial t} = \frac{1}{\tau}(\kappa\widetilde{\delta E}_z - \widetilde{\delta p}_z) - \nu_t k_y^2\widetilde{\delta p}_z - \frac{ik_y}{\rho_{\text{av}}}\widetilde{\delta R}_{yz}, \tag{7c}$$

where $\nu_t = \chi_t/\rho_{\text{av}}$ and $\nu_l = \chi_l/\rho_{\text{av}}$ are the kinematic transport coefficients. As the relaxation phenomena are identical for the x- and z-components, only Equations (7a) and (7b) are treated from here on.

First, we focus on the transverse direction given by Equation (7a). Here two correlation functions are relevant to define, namely, the transverse dipole autocorrelation function (TDACF) and the transverse dipole field cross-correlation function (TDFCCF)

$$C_{pp}^{\perp}(\mathbf{k},t) = \frac{1}{V}\langle\widetilde{\delta p}_x(\mathbf{k},t)\widetilde{\delta p}_x(-\mathbf{k},0)\rangle \tag{8a}$$

$$C_{Ep}^{\perp}(\mathbf{k},t) = \frac{1}{V}\langle\widetilde{\delta E}_x(\mathbf{k},t)\widetilde{\delta p}_x(-\mathbf{k},0)\rangle. \tag{8b}$$

<...> denotes the ensemble avrerage. The dynamics of the TDACF is given by multiplying Equation (7a) with $\widetilde{\delta p}_x(-\mathbf{k},0)$and ensemble averaging

$$\frac{\partial C_{pp}^{\perp}}{\partial t} = \frac{1}{\tau}\left(\kappa C_{Ep}^{\perp} - C_{pp}^{\perp}\right) - \nu_t k^2 C_{pp}^{\perp}, \tag{9}$$

since the stochastic force is uncorrelated with the dipole moment fluctuations, i.e. for all t and $\mathbf{k}$

$$\langle\widetilde{\delta R}_{yx}(\mathbf{k},t)\widetilde{\delta p}_x(-\mathbf{k},0)\rangle = 0. \tag{10}$$

At a moment in time the microscopic configuration of the dipoles yields a corresponding electric field. Recall, no external field is present. The dipoles will align with the local field with the dipole relaxation time τ. For sufficiently high temperature, the thermal perturbations will rapidly change the microscopic configuration leading to a different electric field on a time scale smaller than the dipoles' alignment time. That is, the dipole moment is not affected by the electric field at earlier times for large kinetic energy compared to the electric potential energy. In this limit we have

$$\frac{\partial C_{pp}^{\perp}}{\partial t} = -\left(\frac{1}{\tau} + \nu_t k_y^2\right)C_{pp}^{\perp}. \tag{11}$$

The general solution to Equation (11) is

$$C_{pp}^{\perp}(\mathbf{k},t) = C_{pp}^{\perp}(\mathbf{k},0)e^{-(1/\tau+\nu_t k_y^2)t}. \tag{12}$$

The k_y^2-dependency is a fingerprint of a diffusive process.[6]

It is informative to work in the frequency domain rather than in the time domain. To achieve this Equation (12) is Fourier–Laplace transformed

$$\widehat{C}_{pp}^{\perp}(\mathbf{k},\omega) = \int_0^{\infty} C_{pp}^{\perp}(\mathbf{k},t)e^{-i\omega t}\mathrm{d}t = \frac{(\omega_p^{\perp} + i\omega)C_{pp}^{\perp}(\mathbf{k},0)}{\omega_p^{\perp 2} + \omega^2}, \tag{13}$$

where $\omega_p^{\perp}$ is the transverse peak frequency

$$\omega_p^{\perp} = 1/\tau + \nu_t k_y^2. \tag{14}$$

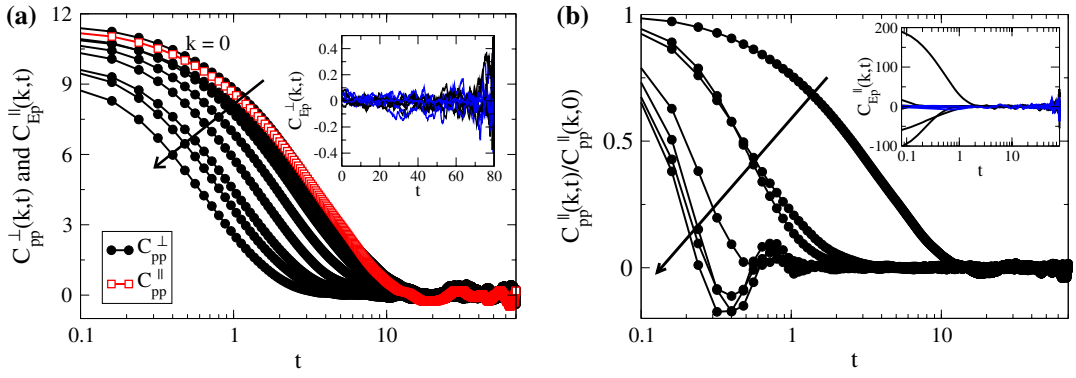

Figure 1. (Color online) The dumbbell system for $q = 5$. (a) The TDACF for different wave vectors. For zero wave vector the LDACF is also shown for comparison. Arrow indicates increasing wave vector. Inset: q=6. The TDFCCF for different wave vectors; black line is the real part, blue broken line the imaginary part. (b) Normalized LDACF for different wave vectors. As in (a) arrow indicates increasing wave vector. Inset: q=6. The LDFCCF for different wave vectors; black line is the real part, blue broken line the imaginary part.

The peak frequency for the TDACF is thus determined by two mechanisms: the wave vector independent dielectric relaxation mechanism and a term which is quadratic with respect to wave vector, i.e. a diffusion mechanism.

One can also define a longitudinal dipole autocorrelation function (LDACF) given by

$$C_{pp}^{\parallel}(\mathbf{k},t) = \frac{1}{V}\langle \widetilde{\delta p}_y(\mathbf{k},t)\widetilde{\delta p}_y(-\mathbf{k},0)\rangle. \tag{15}$$

The dynamical equation for the LDACF is found by multiplying Equation (7b) with $\widetilde{\delta p}_y(-\mathbf{k},0)$ and ensemble averaging. Assuming that the longitudinal dipole field cross-correlation function (LDACF) is zero, i.e.

$$C_{Ep}^{\parallel}(\mathbf{k},0) = \frac{1}{V}\langle \widetilde{\delta E}_y(\mathbf{k},t)\widetilde{\delta p}_y(-\mathbf{k},0)\rangle = 0 \tag{16}$$

we get

$$C_{pp}^{\parallel}(\mathbf{k},t) = C_{pp}^{\parallel}(\mathbf{k},0)e^{-(1/\tau+(\nu_l+\nu_t)k_y^2)t}. \tag{17}$$

The corresponding longitudinal peak frequency in the spectrum of the LDACF is found to

$$\omega_p^{\parallel} = 1/\tau + (\nu_l + \nu_t)k_y^2. \tag{18}$$

3. Molecular simulation results

Two dielectric materials are simulated using molecular dynamics (MD). The first material is a model dielectric composed of diatomic molecules (or dumbbells). Each atom in the dumbbell has charge $\pm q$ and is connected with the other atom through a harmonic spring force. The zero-force length of the spring is 1σ and the spring constant is 1000 $(m\sigma)^2/\epsilon$, where σ is a characteristic length scale, m is the mass and ϵ the energy scale. From here on the physical quantities for this dumbbell material is given in reduced MD units, e.g. temperature is $T^* = Tk_B/\epsilon$. The asterisk will also be omitted. The atoms not belonging to the same molecule interact through the repulsive Weeks–Chandler–Andersen potential [13] and Coulomb potential. The state point is (T, ρ)= (1.0, 0.5) and q varies from $\pm1, \pm2, \ldots, \pm6$. The pressure is positive for all systems. The second dielectric material is liquid water at state point (T, ρ)= (312 K, 998 kg m^{-3}). The water model is the flexible SPC/Fw, see Refs. [14,15] for details. Note, for the water the van der Waal interaction is modelled using the full Lennard–Jones potential with a cut-off of $r_c = 7.9$ Å. Both systems are simulated in a cubic box of length L with the seplib MD library [16] in the NVT ensemble using a Nosé–Hoover thermostat. [17,18] Four hundred molecules are simulated for the dumbbell system, and for water 216 molecules are used. Note that the number of water molecules is the same as in Ref. [15] and finite size effects are negligible.

To reduce the computational time, the electrostatic force calculation is approximated with the shifted force, i.e.

$$\mathbf{F}_c = \frac{q_i q_j}{4\pi\epsilon_0}\left(\frac{1}{r_{ij}^2} - \frac{1}{r_c^2}\right)\frac{\mathbf{r}_{ij}}{r_{ij}} \quad \text{if } r_{ij} \le r_c\,, \tag{19}$$

where ϵ_0 is the free space permittivity, $\mathbf{r}_{ij}$ is the vector of separation between atom i and j, r_{ij} is the norm of $\mathbf{r}_{ij}$ and r_c is the cut-off. For the dumbbell system $r_c = 2.5$ and for water $r_c = 9.16$ Å. For non-confined systems, the shifted-force approximation performs surprisingly well [19,20] and is applicable here.

First results for the dumbbell system are presented and discussed. To first order in the fluctuations the dipole moment per unit mass is

$$\delta\mathbf{p}(\mathbf{r},t) = \frac{1}{\rho_{\text{av}}}\sum_i \boldsymbol{\mu}_i(t)\delta(r - \mathbf{r}_i). \tag{20}$$

In Fourier space with wave vector $\mathbf{k} = (0, k_y, 0)$ one has

$$\widetilde{\delta\mathbf{p}}(\mathbf{k},t) = \frac{1}{\rho_{\text{av}}}\sum_i \boldsymbol{\mu}_i(t)e^{-ik_y r_{y,i}}, \tag{21}$$

with $k_y = 2\pi n/L$, and $n = 0, 1, \ldots$. Using Equation (21) both the TDACF, $C_{pp}^{\perp}$ and LDACF, $C_{pp}^{\parallel}$, are evaluated directly from Equations (8a) and (15).

Figure 1(a) shows the TDACF for different wave vectors for the dumbbell system where $q = 5$. The LDACF for $k_y = 0$ is also shown for comparison. In agreement with the theory, the relaxation of the TDACF is exponential and, furthermore, for zero wave vector the TDACF and the LDACF are almost, but not completely, identical. The relaxation of both the transverse and longitudinal directions are thus to a good approximation given by the same dipole relaxation time at zero wave vector in accordance

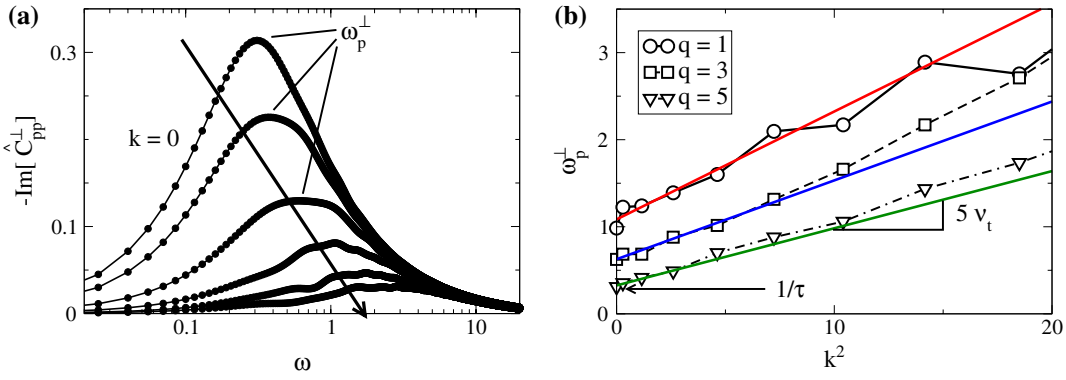

Figure 2. (Color online) The dumbbell model. (a) Imaginary part of the spectrum of the TDACF for different wave vectors, $q = 5$. Arrow indicates increase wave vector. (b) Peak frequency as a function of k_y^2 for different q. Lines are best fit to data for the four lowest wave vectors.

with Equations (12) and (17). Compared to the TDACF, the LDACF features more complicated relaxation for non-zero wave vector, see Figure 1(b). Note, the data are normalized for clarity. For large wave vector oscillatory decay is observed which is not in agreement with the simple exponential decay predicted by the theory. This behaviour is addressed in the following.

In the theoretical treatment it is assumed that the thermal perturbations occur on a smaller time scale than τ. That is, the cross correlation between the dipole moment fluctuations and the electric field fluctuations is zero. To test whether this assumption is valid for the dumbbell system the TDFCCF, $C_{Ep}^\perp$, and LDFCCF, $C_{Ep}^{||}$, are evaluated from Equations (8b) and (16). To this end, the electric field $\delta\mathbf{E}$ is calculated directly from the definition of the field

$$\delta\mathbf{E}(\mathbf{r},t) = \frac{1}{4\pi\epsilon_0}\sum_i \frac{q_i}{r^2}(\mathbf{r}-\mathbf{r}_i). \tag{22}$$

i runs over all atoms with position $\mathbf{r}_i$, and $r^2 = |\mathbf{r}-\mathbf{r}_i|^2$. Space is discretised into an $N\times N\times N$ grid such that $\mathbf{r} = (x_n, y_m, z_l)$, where $n, m, l = 1, 2, \ldots N$; here N is even. The grid spacing is then $\Delta_g = L/N$. The discrete Fourier transform [21] is

$$\widetilde{\delta\mathbf{E}}(k_y,t) = \sum_{n=1}^{N}\sum_{m=1}^{N}\sum_{l=1}^{N}\delta\mathbf{E}(x_n,y_m,z_l,t)e^{-ik_y y_n}(\Delta_g)^3. \tag{23}$$

According to the sampling theorem [21] the wave vectors one can sample is limited to $k_y = 2\pi k/(N\Delta_g)$, where $k = -N/2, \ldots, N/2$. Since the Fourier spectrum is symmetric around $k = 0$, only $k = 0, \ldots, N/2$ are considered here. Also, $y_m = (m-1)\Delta_g$ and one has

$$\widetilde{\delta\mathbf{E}}(k_y,t) = (\Delta_g)^3\sum_{m=1}^{N} e^{-2\pi k(m-1)i/N}\left[\sum_{n=1}^{N}\sum_{l=1}^{N}\delta\mathbf{E}(x_n,y_m,z_l,t)\right]$$
$$k = 0, 1, \ldots \frac{N}{2}. \tag{24}$$

From Equations (24) and (21) one can evaluate the relevant cross correlation functions. The number of grid points is set to $N = 20$ and 40 giving the same qualitative results and data for $N = 40$ is shown in order to obtain the best wave vector resolution.

The insets in Figure 1(a) and (b) show the TDFCCF and LDFCCF for $q = 6$ which correspond to the highest molecular dipole moment studied here. Within the signal-to-noise ratio no cross coupling is observed in the case of the TDFCCF in agreement with the assumption made in the theory section. However, this is not the case for the LDFCCF. Thus, Equation (16) does not hold for the dumbbell system and the prediction for the relaxation Equation (17) and the longitudinal peak frequency Equation (18) will likely fail for this material as also observed in Figure 1(b). Therefore, in the following only the transverse mode is treated.

According Equation (14) the transverse peak frequency $\omega_p^\perp$ is linear with respect to k_y^2. As this result is based on the balance equation, Equation (1), this only holds for sufficiently small wave vectors. The prediction is compared with the spectrum of the TDACF MD data. Figure 2(a) shows an example of the imaginary part of the spectrum for $q = 5$; the arrow indicates increasing wave vector. Also, the peak frequency $\omega_p^\perp$ is indicated for the three lowest wave vectors.

In Figure 2(b) $\omega_p^\perp$ is plotted as a function of k_y^2. Lines are best fit to data using only the four lowest data points. The linear dependency is clearly observed for low wave vector in agreement with the theory. From Figure 2(b) τ can be found from the intercept with the y-axis and the slope gives ν_t. For $q = 1$ one obtains $\tau = 0.9$ and $\nu_t = 0.12$ which is in good agreement with the NEMD results from [7], where $\tau = 1.1$ and $\nu_t = 0.11$. It is worth noting that the larger the dipole moment, the lower the transport coefficient ν_t. This is likely caused by a reduced molecular diffusivity, which is one mechanism responsible for the dipole flux.

In general the peak frequency is given by some function of wave vector, i.e. $\omega_p^\perp = \omega_p^\perp(k_y)$. It is assumed that $\omega_p(k_y)$ has a

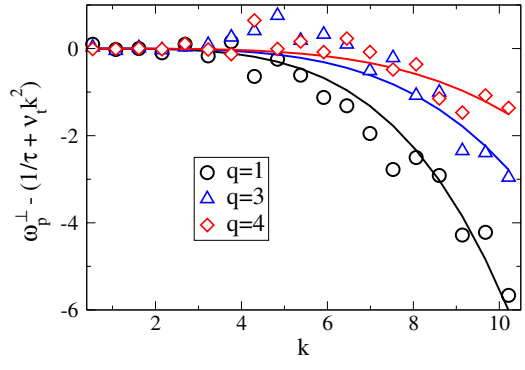

Figure 3. (Color online) Dumbbell model. Deviation of the peak frequency from the theoretical predictions, Equation (14). Full lines are best fits of $f(k) = c_4 k$ to points.

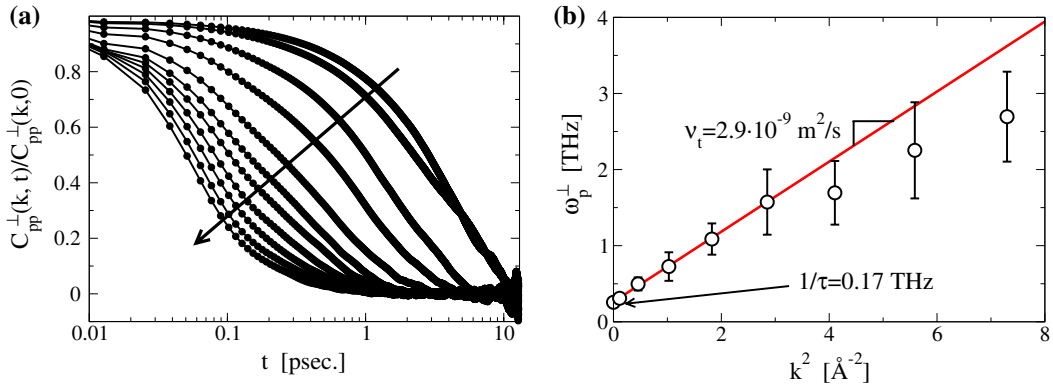

Figure 4. (Color online) Liquid water. (a) Normalised TDACF. Arrow indicating increasing wave vector. (b) Transverse peak frequency $\omega_p^{\perp}$ as a function of k_y^2. Line is the best fit to the data points for the four lowest wave vectors.

Taylor expansion around $k_y = 0$. The odd terms must be zero as $\omega_p^{\perp}$ is symmetric around $k_y = 0$ and one has

$$\omega_p^{\perp}(k_y) = 1/\tau + \nu_t k_y^2 + \frac{\nu_{t,4}}{4!}k_y^4 + \frac{\nu_{t,6}}{6!}k_y^6 + \ldots \tag{25}$$

where

$$\nu_{t,n} = \left.\frac{\mathrm{d}^n \omega_p^{\perp}}{\mathrm{d}k_y^n}\right|_{k_y=0}, \tag{26}$$

and $\nu_t = \frac{\nu_{t,2}}{2!}$. Figure 3 shows a plot of the deviation of the peak frequency from the theoretical prediction for different charges and wave vectors. The full lines are best fits of $f(k) = c_4 k^4$ to data. The fits primarily serve as a guide to the eye, but also indicate that the peak frequency can be approximated by a fourth-order Taylor approximation over a large range of wave vectors since $\omega_p^{\perp} \approx 1/\tau + \nu_t k_y^2 + \nu_{t,4} k_y^4/4!$, where the fourth-order coefficient must be $\nu_{t,4} \approx 4! c_4$.

The TDACF, Figure 4(a), and the transverse peak frequency, Figure 4(b), for liquid water are investigated. As expected, the diffusive fingerprint, $\omega_p^{\perp} \propto k_y^2$, is observed for small wave vectors. The dipole relaxation time is found to be $\tau \approx 6$ psec. This value disagrees somewhat with the Debye relaxation time, $\tau_D = 9.50$ psec. for the flexible water model SPC/Fw.[15] The Debye relaxation time is found from the total dipole moment relaxation function [15] and is equivalent to the method used here for zero wave vector. The kinetic transport coefficient is $\nu_t = 2.9 \times 10^{-9}$ m^2/s.

As mentioned above, Hansen [7] studied the dielectric response in the presence of an external spatially varying electric field. The relative response reduction due to the dipole diffusion mechanism can be measured directly through the dimensionless number [7]

$$Je = k_y^2 \nu_t \tau \geq 0. \tag{27}$$

For the state point studied here $Je = k_y^2 1.7 \times 10^{-20}$ m^2. This leads to a 10% dielectric response reduction for wave length of 2.6 nm.

4. Conclusion

Here the transverse and longitudinal dipole autocorrelation functions where studied by comparing theoretical predictions with EMD simulation data. In the limit of small wave vector, the peak frequencies for the corresponding spectra are determined by the wave vector-independent dielectric relaxation and a quadratic wave vector-dependent diffusion mechanism. It was shown that for the transverse relaxation the coupling to the electric field can be ignored, but this is not the case for the longitudinal relaxation. The underlying mechanism for this coupling is not clear.

Evaluation of the TDACF provides an EMD method to evaluate the dielectric relaxation time and the transport coefficient governing the diffusion process. From these two parameters an estimate of the non-equilibrium dielectric response can be given through the dimensionless number *Je*.

Disclosure statement

No potential conflict of interest was reported by the author.

Acknowledgements

The author wishes to thank Lundbeckfonden for supporting this work as part grant no. R49-A5634. The centre for viscous liquid dynamics 'Glass and Time' is sponsored by the Danish National Research Foundation (DNRF).

References

[1] Luzar A, Svetina S, Zeks B. Consideration of the spontaneous polarisation of water at the solid/liquid interface. J. Chem. Phys. 1985;82:5146–5156.
[2] Valleau JP, Gardner AA. Water-like particles at surface. 1. The uncharged, unpolarizable surface. J. Chem. Phys. 1987;86:4162–4170.
[3] Bonthuis JD, Gekle S, Netz RR. Dielectric profile of interfacial water and its effect on double-layer capacitance. Phys. Rev. Lett. 2011;07:166102.
[4] Yeh I-C, Berkowitz ML. Ewald summation for systems with slab geometry. J. Chem. Phys. 1999;111:3155–3162.
[5] Bresme F, Lervik A, Bedaux D, et al. Water polarisation under thermal conditions. Phys. Rev. Lett. 2008;101:020602.
[6] Hansen JP, McDonald IR. Theory of simple liquids. Amsterdam: Academic Press; 2006.
[7] Hansen JS. Reduced dielectric response in spatially varying electric fields (forthcoming). 2015.
[8] del Castillo LF, Dávalos-Orozco LA. Dielectric relaxation in polar and viscoelastic fluids. J. Chem. Phys. 1990;93:5147–5156.
[9] Dahler JS, Scriven LE. Theory of structured continua I. General considerations of angular momentum and polarisation. Proc. R. Soc. Lond. A. 1963;27:504–527.

[10] Hansen JS, Dyre JC, Daivis JP, et al. Continuum nanofluidics. Langmuir. Forthcoming 2015.
[11] de Zárate JMO, Sengers JV. Hydrodynamic fluctuations. Amsterdam: Elsevier; 2006.
[12] de Groot SR, Mazur P. Non-equilibrium thermodynamics. New York (NY): Dover Publications; 1984.
[13] Weeks JD, Chandler D, Andersen HC. Role of repulsive forces in determining the equilibrium structure of simple liquids. J. Chem. Phys. 1971;54:5237–5247.
[14] Toukan K, Rahman A. Molecular-dynamics study of atomic motions in water. Phys. Rev. B. 1985;31:2643–2648.
[15] Wu Y, Tepper HL, Voth GA. Flexible simple point-charge water model with improved liquid-state properties. J. Chem. Phys. 2006;124:024503.
[16] Hansen JS. [cited 2015] Available from: https://code.google.com/p/seplib/.
[17] Nosé S. A molecular dynamics method for simulation in the canonical ensemble. Mol. Phys. 1984;52:255–268.
[18] Hoover WG. Canonical dynamics: equilibrium phase-space distributions. Phys. Rev. A. 1985;31:1695–1697.
[19] Hansen JS, Schrøder TB, Dyre JC. Simplistic Coulomb forces in molecular dynamics: comparing the Wolf and shifted-force approximations. J. Phys. Chem. B. 2012;116:5738–5743.
[20] Takahashi KZ, Narumi T, Yasouko K. Cutoff radius effect of the isotropic periodic sum and Wolf method in liquid-vapor interfaces of water. J. Chem. Phys. 2011;34:174112.
[21] Press WH, Vettering WT, Teukolsky SA, et al. Numerical recipes in C. Cambridge: Cambridge University Press; 1992.